PAPER

Modeling and Control of the MARES Autonomous Underwater Vehicle

AUTHORS

Bruno Ferreira
Aníbal Matos
Nuno Cruz
Miguel Pinto
INESC Porto,
University of Porto

ABSTRACT

In this work, we address the modeling and control problems in the domain of underwater vehicles. We focus on a prototype of an autonomous underwater vehicle. Although the work presented here is applied to a particular vehicle with four controllable degrees of freedom, the method may be easily extended to several submerged bodies. In the engineering area, modeling of systems is done frequently, as it yields a mathematical translation of their behavior. Since models can become an important tool to solve problems related to its motion or even to the design of controllers, we obtain a model with six degrees of freedom for such a vehicle.

Robust control of underwater vehicles is an area in which many efforts were applied over the last two decades. However, due to nonlinear dynamics, it may be hard to design robust controllers that yield the expected behavior, and there is no general procedure to develop them. Here, we propose an approach that combines nonlinear controllers based on the deduced model and on the Lyapunov theory to control the velocities of the vehicle with linear controllers that control the vehicle's position. We derive control laws to perform several maneuvers, both in the vertical and the horizontal planes, in a decoupled way, which is made possible through the configuration of thrusters. Finally, we present realistic simulations and experimental results that validate the proposed approach in the definition of the control laws.

Keywords: Modeling, Nonlinear control, Autonomous underwater vehicle, Hydrodynamics, Maneuvering

1. Introduction

1.1. Motivation

Autonomous underwater vehicles (AUVs) are robotic systems whose applications are becoming wider in several domains, such as environmental monitoring, underwater intervention and oceanography. Currently, several AUVs are commercially available and a multitude of prototypes have been implemented by researchers, responding to challenges in a large amount of fields. In these, adequate control of the vehicle is of the utmost importance so as to guarantee good behavior during its operation.

In the last few decades, modeling has become an important method to analyze systems without the need for implementation. The popularity of this method has increased as systems became more complex and as the implementation and testing became more expensive and subject to several constraints. On the other hand, computational tools are increasingly more powerful and have reached a point in which simulation of very complex systems is very realistic. Moreover, models are also very important in the design of controllers and are often used as a basis for their design.

Control is an important domain in engineering and aims at modifying a system to make it operate adequately. For the particular case of vehicles, control is of the utmost importance since the inputs of the system have to be computed so that the vehicle executes the required maneuvers. In this case, the greater the autonomy of the vehicles, the more critical is the need for robust controllers. Here, autonomy is defined as the capability to perform actions without the need for external commands. However, the determination of control laws requires a careful analysis of the system to guarantee that the vehicle is operated correctly.

In this work, we address the design of the control system for an AUV with nonlinear dynamics. Our approach is based on the decoupling of horizontal and vertical motions of the vehicle and on the design of nested control loops for each plane. The design of the controllers follows a systematic approach and is based on a dynamic model of the vehicle.

The main contributions of this work are the complete procedure to derive controllers for nonlinear systems and the experimental demonstration of the robustness of such implementation. Although the results presented here are focused in a specific underwater vehicle, the method may be

easily extended to other vehicles or even to totally different systems. Since it is quite generic, the method is a good candidate for applications in both linear and nonlinear domains but may imply the use of a fairly accurate model.

1.2. Modeling and Control of AUVs

The mathematical formulation of the dynamics of a submerged vehicle has its foundation in classic mechanics and in the identification of all forces that actuate on the body. Besides inertial and gravitational forces, hydrodynamic related forces, such as added mass, drag or restoring forces, among others, play an important role here (Fossen, 1995; Prestero, 2001). The determination of such forces and torques is many times based on semi-empirical and empirical formulas obtained from experiments (Hoerner, 1965; Prestero, 2001) and depends mostly on the geometric shape and roughness of the hull. Thus, accurate models are difficult to obtain and are affected by various uncertainties. Moreover, some effects of the fluid on the vehicle are often neglected or are not even considered during the modeling process, as is the case of the counter-intuitive Munk moment (Triantafyllou and Hover, 2003; Tyagi and Sen, 2006), for instance.

Control of AUVs has been addressed by many authors in the literature (Healey and Lienard, 1993; Fossen, 1995; Prestero, 2001; Silvestre et al., 2002; Evans and Nahon, 2004; Aguiar and Hespanha, 2007; Matos and Cruz, 2009). Since the dynamic model is nonlinear, control laws are not obvious, and common linear techniques (Ogata, 1997) may be inadequate in a large range of operations. Several methods have been used, such as machine learning methods (van de Ven et al., 2005), linear control laws for a narrow range of operation (Prestero, 2001), nonlinear Lyapunov-based design methods (Aguiar and Hespanha, 2007; Li et al., 2009), sliding mode control methods (Healey and Lienard, 1993; Song et al., 2002) or even nonlinear model predictive control (Dunbar and Murray, 2002). Gain-scheduled techniques (Silvestre et al., 2002), which combine a family of linear controllers for nonlinear systems, have also been used. However, since they require linearization on several points of operation and the consideration of several interpolated linear controllers that operate on different subsets of system states, the total number of gain-scheduled controllers may easily increase. Indeed, the use of a too reduced number of linear controllers may deteriorate the response or even make the system unstable, since stability is only guaranteed in the vicinity of the linearization point (Aguiar and Hespanha, 2004). Machine learning methods such as artificial intelligence have been used in the control of AUVs as well. Van de Ven et al. (2005) presented three main topologies of neural networks for control, which consist essentially of learning the actuation values according to the states of the vehicle and command (both as inputs of the neural network) (Yuh, 1994), in an inverse model of the vehicle or in a compensation of a conventional controller. Prestero (2001) has tested a linear control law for a constant forward velocity, which results in good performance. However, for large range of operation, this linearization is no longer accurate and, consequently, the controllers' performance is degraded. Li et al. (2009) has applied the backstepping theory to a surface vehicle with four degrees of freedom (DOF) considering several simplifications of its hydrodynamic model. Backstepping methods are successfully applied by Aguiar and Hespanha (2007), who considers the six DOF of an underactuated autonomous vehicle.

Several authors (Fossen, 1995; Prestero, 2001; Aguiar and Hespanha, 2007) address control problems using a reduced model of the vehicle. However, there is a tradeoff between model simplification and accuracy. Oversimplified models may lose accuracy, and their application in control may be limited due to unmodeled effects, which results in lack of robustness or even stability. On the other hand, the design of control laws for too complex models can be a hard task with a minor performance gain. Thus, it is common to "split" the model in two or more decoupled models in terms of motion (Aguiar and Hespanha, 2007), thus obtaining less complex control laws.

1.3. Proposed Approach: Overview

In this work, we consider a model with six DOF of the Modular Autonomous Robot for Environment Sampling (MARES) AUV, taking into account that control laws derivation assumes the use of mathematical translation of the dynamics. In section 2, we present the vehicle as well as the kinematics fundamentals and the specific modeling process. Some geometric characteristics are used to simplify the expressions of forces, without any loss of accuracy. Unlike Li et al. (2009), no simplification of the nonlinear model will be performed at this stage.

In section 3, we present the design of controllers using the previously obtained model. We start by deriving different velocity controllers for both horizontal and vertical motion. Control

laws are based on the Lyapunov theory to assure stability in the required operation range. Then, we move on to the derivation of the position controllers. Adequate definitions of errors are presented, and linear control laws are obtained. Here, a configuration using velocity controllers in an inner loop and position controllers in an external loop is proposed. We present different controllers for vertical control, line following and immobilization in the water column.

In section 4, we present the results of the implementation of the controllers through simulations and experiments. There we try to validate and analyze the performance and the accuracy of controllers under real conditions.

2. Modeling

In this section, we present a general method to determine a model for a body inserted in a fluid. We start by presenting the AUV MARES and continue with the rigid body dynamic and with the definition of forces that actuate on the vehicle. Finally, we present the general expression of the dynamic.

2.1. MARES Autonomous Underwater Vehicle

MARES (Cruz and Matos, 2008; Matos and Cruz, 2009) is a 1.5-m-long AUV designed and built by the Ocean Systems Group at the Faculty of Engineering of University of Porto. MARES has a slender body form and is endowed with four thrusters that confer it four controllable DOF. Each thruster may deliver up to 22 N of force. It can dive up to 100 m deep and, unlike similar-size systems, it has vertical thrusters that enable purely vertical motion in the water column. Forward velocity may be independently defined, from 0 to about 2 m/s, through the regulation of horizontal thruster forces.

Though MARES can have multiple configurations, we will only assume the one presented in Figure 1.

FIGURE 1

MARES AUV ready for an autonomous mission.

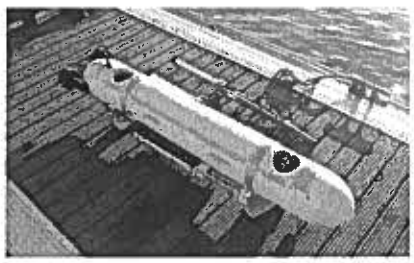

In Table 1, we present the main dimensions of MARES.

2.2. Kinematics

To simplify the deduction of model expressions, we consider earth-fixed and body-fixed reference frames (Siegwart and Nourbakhsh, 2004). Both are orthogonal. We assume that the earth-fixed frame, formed by the axes set $\{x, y, z\}$, does not experience any acceleration, i.e., it is inertial. The body-fixed orthogonal reference frame is formed by $\{x_B, y_B, z_B\}$, and its origin coincides with the center of gravity. We consider that x_B is the axis along the body, pointing in the same direction of the nose, while y_B is the lateral axis and z_B is the vertical axis that points down (in the same direction of vertical thrusters inserted in the hull).

A linear vector $c_B \in \mathbb{R}^3$ in the body-fixed reference frame may be expressed in the earth-fixed frame through the relation

$$c = J(\eta) \cdot c_B \tag{1}$$

where $\eta = [x\ y\ z\ \varphi\ \theta\ \psi]$ is the absolute position vector, $J \in \mathbb{R}^{3\times3}$ is the rotation matrix of the referential $\{x, y, z\}$ from $\{x_B, y_B, z_B\}$. Symbols φ, θ and ψ represent the roll, pitch and yaw angles, respectively. Note that J is orthonormal and its inverse is given by $J^{-1} = J^T$.

2.3. Rigid Body Dynamic

Newton's second law states that a rigid body at rest only experiences motion if a force is applied to it. In the inverse case, a body only reaches the rest state if a force counters its motion. Mathematically, these concepts are translated by the two classical expressions of the conservation of linear and angular momentum.

Before deducing the AUV model, we should define some variables: r and r_G are the position of a point of the body related to the earth-fixed

TABLE 1

Dimensions of MARES.

Parameter	Value	Description
l	$1.41 \cdot 10^{0}$ m	Hull length
d	$2.00 \cdot 10^{-1}$ m	Hull diameter (cylinder)
W	$3.14 \cdot 10^{2}$ N	Weight
B	$3.16 \cdot 10^{2}$ N	Buoyancy
F	22 N	Maximum force of each thruster

inertial frame and related to the body-fixed frame; $\upsilon_r = [u\ v\ w\ p\ q\ r]^T$ is the velocity vector in the body-fixed referential frame. Components u, v, w represent the linear velocities along the surge, sway and heave, while p, q, r are the angular velocities along roll, pitch and yaw, respectively.

The development of both equations for the conservation of linear and angular momentum gives the sum of external forces and moment that actuate on the body, respectively:

$$\sum f_{ext} = m(\dot{\upsilon}_r + \omega_B \times \upsilon_B + \dot{\omega}_B \times r_G + \omega_B \times (\omega_B \times r_G)) \quad (2)$$

$$\sum m_{ext} = mr_G \times \dot{\upsilon}_r + mr_G \times (\omega_B \times \upsilon_B) + I_B \dot{\omega}_B + \omega_B \times (I_B \omega_B) \quad (3)$$

where $\sum f_{ext} = (\sum X_{ext}, \sum Y_{ext}, \sum Z_{ext})^T$ is the vector of force components in x_B, y_B and z_B axes, $\sum m_{ext} = (\sum K_{ext}, \sum M_{ext}, \sum N_{ext})^T$ is the vector of moment components along x_B, y_B and z_B axes, m is the mass of the vehicle, I_B is the inertia tensor with respect to the body-fixed origin, $\dot{\upsilon}_r$ is the time derivative of the velocity in the body-fixed frame, υ_B and ω_B are linear and angular velocities of the body in the earth-fixed frame, respectively, $\dot{\upsilon}_B$ and $\dot{\omega}_B$ their time derivative and × represents the cross product.

In underwater vehicle modeling, it is common practice to consider the origin of the body-fixed referential frame that is coincident with the center of gravity, $r_G = [0\ 0\ 0]$. Indeed, it simplifies several expressions of the dynamics model.

The deduction of and may be consulted in Fossen (1991). Designating $\tau_{ext} = [\sum f_{ext}\ \sum m_{ext}]^T$ as the vector of forces and moments, we may write

$$\tau_{ext} = M_{RB}\,\dot{\upsilon}_r + C_{RB}(\upsilon_r)\,\upsilon_r \quad (4)$$

where $M_{RB}, C_{RB}(\upsilon_r) \in \mathbb{R}^{6\times6}$ are the rigid body inertia matrix and the Coriolis and centrifugal terms matrix, respectively. These two matrices depend on the vehicle mass and on the moments of inertia, as presented in the Appendix.

2.4. Hydrodynamic

A body inserted in a fluid experiences several forces. In the particular case of underwater vehicles, these forces are due to

- added mass, originated by the acceleration of involving particles of fluid during the acceleration of the body;
- drag, due to friction on the boundary layers, pressure on the hull and vortices created by non null velocity;
- potential damping that is originated by non-null velocity of the body. Its contribution is small compared to drag and is often included in it, as will be done in this paper;
- Froude-Krylov force due to the acceleration of the fluid;
- restoring forces due to the weight and to the buoyancy; and
- propulsion applied by actuators.

Note that forces induced by the wind and by waves are neglected, assuming that, for underwater vehicles moving sufficiently far from the surface, these effects are relatively small. On the other hand, Froude-Krylov forces are neglected in the presented model due the reduced variation of the fluid current velocity in the environments where MARES performs operations (river, calm ocean).

Force coefficients are not determined in this paper for simplicity. Their deduction may be consulted in Ferreira et al. (2009).

2.4.1. Added Mass

The symmetry of the MARES AUV relative to the plane formed by $\{x_B, z_B\}$ makes it possible to simplify the added mass force expression that is given by

$$\tau_A(\dot{\upsilon}_r, \upsilon_r) = -M_A \dot{\upsilon}_r - C_A(\upsilon_r)\,\upsilon_r \quad (5)$$

where $M_A, C_A(\upsilon_r) \in \mathbb{R}^{6\times6}$ are the added mass matrix and Coriolis and centrifugal terms matrix, respectively.

To clarify the simplification method, we consider the following examples:

- Linear acceleration after the x_B axis does not generate any moment along z_B, which implies that the corresponding term in M_A must be null ($N_{\dot{u}} = 0$).
- Angular acceleration along the y_B axis will not have any influence on the force along the same axis.
- Linear acceleration after z_B does not create any force along x_B or y_B axis.

Extending the same reasoning to others terms, we obtain the matrices M_A and C_A presented in the Appendix. More cases are exposed by Fossen (1995) for the simplification of different planes of symmetry.

It is important to refer that coefficients like $Y_{\dot{r}}, Z_{\dot{q}}, M_{\dot{w}}$ and $N_{\dot{v}}$ are non-null due to the asymmetry relative to $\{y_B, z_B\}$ plane. The sonar hull, on the lower part of MARES (cf. Figure 2), turns the body asymmetric after the $\{x_B, y_B\}$ plane, making the coefficients $X_{\dot{q}}, Y_{\dot{p}}, K_{\dot{v}}, M_{\dot{u}}$ non-null. It should be noted that the model does not lose accuracy since all asymmetries are considered.

FIGURE 2

Superior (top) and lateral view of MARES.

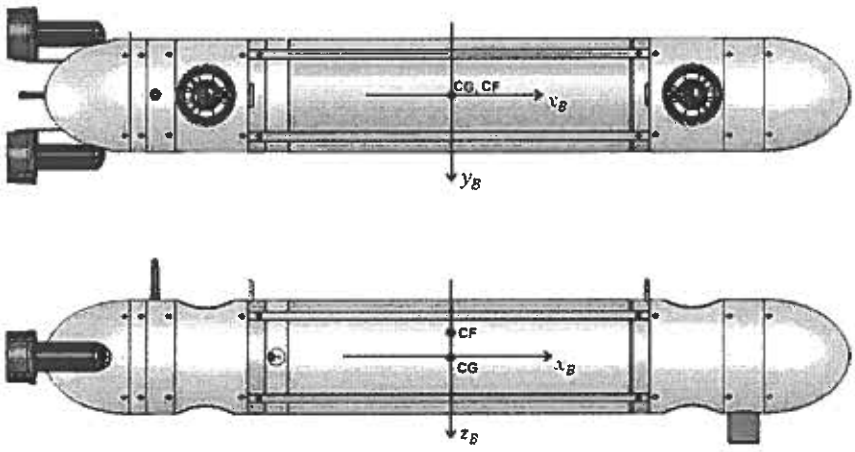

2.4.2. Viscous Hydrodynamic Forces

Drag forces are generally expressed by a high order polynomial equation (Fossen, 1995). However, for the considered range of velocities ($0.5 \leq u \leq 2.5$ m/s), the quadratic term is dominant. This assumption makes it possible to write the drag forces and moments vector as

$$\tau_V(v_r) = -D_V(v_r)\, v_r \tag{6}$$

where $D_V(v_r) \in \mathbb{R}^{6\times 6}$.

As in the case of added mass terms, symmetry related to the $\{x_B, z_B\}$ plane allows simplification of D_V. Extending the simplification method of Fossen (1991) to viscous hydrodynamic force contributions, several coefficients may be dropped. For example, motion on the y_B-axis will originate a moment along z_B (yaw moment). On the other hand, the same motion will not influence the linear motion along x_B and z_B or the angular motion along y_B (pitch moment). Applying the same reasoning for the remaining coefficients, one can simplify the drag matrix D_V as shown in the Appendix.

2.4.3. Restoring Forces

As stated before, these forces result from the weight and the buoyancy and are given in modulus by W and B, respectively. The expression of restoring forces is given by

$$\tau_C(\eta) = -\begin{bmatrix} J^{-1}\begin{bmatrix} 0 \\ 0 \\ W - B \end{bmatrix} \\ r_G \times \left(J^{-1}\begin{bmatrix} 0 \\ 0 \\ W \end{bmatrix}\right) - r_{CB} \times \left(J^{-1}\begin{bmatrix} 0 \\ 0 \\ B \end{bmatrix}\right) \end{bmatrix} = -\begin{bmatrix} (W - B)\sin\theta \\ 0 \\ (B - W)\cos\theta \\ 0 \\ -z_{CF}B\sin\theta \\ 0 \end{bmatrix} \tag{7}$$

where r_G and r_{CF} are positions of centers of gravity and buoyancy, respectively, related to the body-fixed frame. We consider that the fixed-body referential coincides with the center of gravity and that $x_{CB} = y_{CB} = 0$. In the case of MARES, we consider that the angle after x_B (roll) is $\varphi \approx 0$, thus translating its real observed behavior.

2.4.4. Propulsion Forces

Defining F_{pi} as the force applied by the i-th thruster, with P_1, P_2, P_3, and P_4 being the horizontal left and right and vertical back and front thruster, respectively, and $f_p = [F_{p1}\ F_{p2}\ F_{p3}\ F_{p4}]^T$ as the vector of forces applied by thrusters, it is possible to write the vector of forces and moments performed by the thrusters as

$$\tau_p = P \cdot f_p \tag{8}$$

where $P \in \mathbb{R}^{6\times 4}$ is the propulsion matrix. Again, its expression may be consulted in the Appendix.

2.5. General Equation of Dynamics

From sections 2.3 and 2.4, the simplified dynamic equation results

$$\tau_{ext} = \tau_A(\dot{v}_r, v_r) + \tau_V(v_r) + \tau_C(\eta) + \tau_p(v_r, n) \tag{9}$$

Substituting vectors by their expressions and manipulating them algebraically, we easily obtain:

$$(M_{RB} + M_A)\dot{v}_r = -[C_{RB}(v_r) + C_A(v_r) + D_V(v_r)]v_r + \tau_C(\eta) + P \cdot f_p \tag{10}$$

2.6. Estimation of Coefficients

Coefficients of the several forces considered are estimated based on semi-empirical and experimental expressions (Fossen, 1995; Prestero, 2001; White, 2008), since theoretical formulas are not available due to the

complexity of hydrodynamics. It is a common practice to use experimental devices to determine the dynamics of immerged bodies, obtaining accurate results for the values of force coefficients. An example of that was the work carried out by Prestero (2001) to determine coefficients of the REMUS AUV using a tow tank. Due to physical constraints, we are not able to perform such experiments accurately, whereby estimation becomes the sole alternative.

Since the task of computing these parameters is quite extensive and is beyond the scope of this paper, we will not determine them here. However, we recommend the reading of Ferreira et al. (2009) for a detailed complete method on the determination of coefficients of added mass and viscous hydrodynamic forces that MARES is subject to. Added mass coefficients depend essentially on the volume of the vehicle while the viscous hydrodynamic forces depend on the projected areas of the vehicle in several planes. A geometric model of the vehicle is considered: the nose and the tail are composed of two semi-ellipsoids and the central part of the body is a cylinder. Propellers are approximated by narrow cylinders as well as the small sonar hull ahead of the vehicle.

3. Control

To perform some maneuvers, an adequate control of MARES AUV is necessary. Using the Lyapunov theory, we will derive feedback control laws, finding an appropriate expression for the inputs of the system-thrusters. In this section, after presenting some of the fundamental concept of Lyapunov stability, we start by presenting the development of vertical and horizontal velocity, followed by position controllers. The latter will make it possible for the vehicle to remain in a determined vertical position, follow an imaginary line and stay motionless in the water column.

The model given in section 2 makes it possible to obtain an approach to the real behavior of MARES. However, it is affected by modeling uncertainties and neglected terms. For the development of controllers, these deviations are considered to be disturbances during the operation of the vehicle.

The control of MARES is performed by actuations of thrusters, whereby, from expression (10), we may conclude that f_p is the control variable. We assume that we can instantly vary the forces of propellers though it is not true in reality. This assumption simplifies the analysis and the determination of controllers and may be justified by the fact that time constants associated to the actuation are much smaller than the ones associated to the vehicle motion. Some controllers are developed combining nonlinear (Slotine and Li, 1991; Khalil, 2002) and linear (Ogata, 1997) controllers.

3.1. Lyapunov Theory

Lyapunov theory is often used in nonlinear systems as in Aguiar and Hespanha (2007). It allows us to draw conclusions on the stability of a system and designing control laws. Authors recommend the reading of Slotine and Li (1991) and Khalil (2002) for a more detailed presentation of the Lyapunov theory.

The Lyapunov direct method is based on the analysis of energy behavior in a system. The major principle is reasoned by the following fact: if the total energy of a system is constantly dissipated along its operation, or motion, it will stabilize in an equilibrium or point, or state. To illustrate this idea, we consider an oscillating pendulum with non-null potential energy. Assuming that there is friction due to oscillation, the amplitude of its motion will reduce gradually until the system stops at the point where the resultant force is zero (equilibrium point where the potential energy is lower).

Before presenting the more useful results from this theory, a few definitions are required:

- A scalar function $f(x)$ is said to be globally positive definite if $f(x) > 0$, $\forall\, x \neq 0$ and globally positive semi-definite if $f(x) \geq 0$, $\forall\, x \neq 0$.
- A scalar function $f(x)$ is said to be globally negative definite if $f(x) < 0$, $\forall\, x \neq 0$, and globally negative semi-definite if $f(x) \leq 0$, $\forall\, x \neq 0$.

A function $V(x)$ is said to be a Lyapunov function of a system if it is positive definite, with continuous partial first derivatives and, in addition, if its time derivative is negative semi-definite ($\dot{V}(x) \leq 0, \forall\, x \neq 0$) for any trajectory of the state x.

The Lyapunov theory states through the global stability theorem that if "there exists a scalar function V of the state x with continuous first derivatives such that $V(x)$ is positive definite, $\dot{V}(x)$ is negative definite and $V(x) \longrightarrow \infty$ as $x \longrightarrow \infty$, then the equilibrium point at the origin is globally asymptotically stable" (Slotine and Li, 1991).

3.2. Velocity Controllers

3.2.1. Vertical Velocity Controller

In this subsection, we will only consider the motion in the vertical plane or, in other words, in the z_B-axis direction and in the pitch angle (cf. Figure 2). To simplify the determination of the vertical velocity controller, we start by reducing the order of the model. This implies that we must

eliminate lines and columns of the equation matrices in equation (10) whose influences on the z_B and pitch motion are negligible. It results in the elimination of the second, fourth and sixth lines and columns of matrices in equation (10). In the vector case, only the same lines are eliminated. Note that the forward velocity u (after x_B-axis) is considered in this case because the model has non-negligible cross terms that influence the vertical motion, as it can be seen in (Ferreira, 2009). Neglecting this velocity component would not be critical, but it would generate a less robust response of the system to disturbances due to forward velocity. Thus, the reduced model result from equation (10)

$$(M_{RBv} + M_{Av})\dot{v}_{rv} = -[C_{RBv}(v_{rv}) + C_{Av}(v_{rv}) + D_{Vv}(v_{rv})]v_{rv} - g_v(\eta) + P_v \cdot f_{pv} \tag{11}$$

where $M_{RBv}, M_{Av}, C_{RBv}, C_{Av}, D_{Vv} \in \mathbb{R}^{3\times3}$, $P_v \in \mathbb{R}^{3\times2}$, $v_{rv}, \tau_{Cv} \in \mathbb{R}^3$ and $f_{pv} \in \mathbb{R}^2$.

We wish to control the linear and angular velocities w and q by actuating in the vertical thrusters $P3$ and $P4$, whereby we define an error vector as follows:

$$e_v = S_v \cdot v_{rv} - v_{refv} = \begin{bmatrix} 0 & 1 & 0 \\ 0 & 0 & 1 \end{bmatrix} \begin{bmatrix} u \\ w \\ q \end{bmatrix} - \begin{bmatrix} w_{ref} \\ q_{ref} \end{bmatrix} = \begin{bmatrix} w - w_{ref} \\ q - q_{ref} \end{bmatrix} \tag{12}$$

where e_v, v_{rv}, $v_{refv} = \left[w_{ref}, q_{ref}\right]^T \in \mathbb{R}^3$ and $S_v = [0_{2\times1}\ diag(1, 1)]$ is the selection matrix, in this case.

Note that the component of the error along surge is considered for reasons that will be clear in the next expressions. With this controller, we are not interested in controlling the surge component of the velocity. Nevertheless, this component has a significant influence on vertical motion, whereby it is considered.

Expression (13) defines the Lyapunov candidate function

$$V = \frac{1}{2} e_v^T e_v \tag{13}$$

whose time derivative results

$$\dot{V} = e_v^T \dot{e}_v = e_v^T (S\dot{v}_{rv} - \dot{v}_{refv}) \tag{14}$$

After the Lyapunov theory, the stability of the system implies $\dot{V}$ that must be negative definite, which leads to impose

$$e_v^T (S\dot{v}_{rv} - \dot{v}_{ref}) < 0 \Rightarrow S_v\dot{v}_{rv} - \dot{v}_{refv} \leq -k_e e_v \tag{15}$$

for some $k_e \in \mathbb{R}, k_e > 0$.

Assuming that we are able to modify the value of the acceleration of MARES along the DOF through the actuation of the thrusters, we impose

$$S_v\dot{v}_{rv} = \dot{v}_{refv} - k_e e_v \tag{16}$$

Substituting equation (16) into the simplified equations (11) and (10) and manipulating algebraically to satisfy equation (15), we obtain

$$-S_v M_v^{-1}(C_{RBv}(v_r) + C_{Av}(v_r) + D_{Vv}(v_r)) \cdot v_{rv} - S_v M^{-1} g_v(\eta) - (\dot{v}_{refv} - k_e e_v) + S_v M^{-1} P_v f_{pv} = 0 \tag{17}$$

assuming that $M_v = M_{RBv} + M_{Av}$ is invertible.

To guarantee that is negative definite satisfying equations (16) and (15), we choose f_p as we show in the following expression, considering that we can actuate directly in this variable:

$$f_p = \left(S_v M_v^{-1} P_v\right)^{-1} \left[S_v M_v^{-1} (C_{RBv}(v_r) + C_{Av}(v_r) + D_{Vv}(v_r)) \cdot v_{rv} + S_v M^{-1} g_v(\eta) + \left(\dot{v}_{refv} - k_e e_v\right)\right] \tag{18}$$

assuming that $S_v M_v^{-1} P_v$ is invertible as in fact it is. This expression gives the closed loop control law for the vertical velocity, with f_p as the control input of the system.

Going back to equation (14) and combining with equation (16), the time derivative of the Lyapunov function results in

$$\dot{V} = -k_e e_v^T e_v < 0, \qquad \forall\, e_v \neq 0 \tag{19}$$

it is possible to prove the global asymptotical stability of the system (Khalil, 2002), as desired.

The determination of the value of k_e depends on actuators characteristics, especially on their saturation value, but not only. This gain is dimensioned so that actuation saturation is not reached during long intervals of time, which could degrade the system's response. In addition, it is convenient to define error saturations to prevent it from reaching the nondesirable saturation. These saturations are determined according to maximum attainable velocities.

However, in most cases, controller gains must be adjusted a posteriori using practical techniques, in particular for nonlinear systems, for which it is difficult to compute response characteristics as overshoot, rising time or settling time.

3.2.2. Horizontal Velocity Controller

As for the previous case, we start by reducing the order of the model in equation (10), reducing the complexity of the controller determination. Only motions along x_B, y_B and yaw are considered (cf. Figure 2). The remaining components are neglected because, according to the model by Ferreira et al. (2009), their influences are relatively small, whereby their inclusion is not justified and they are considered as disturbances. This implies that the third, fourth and fifth line and columns of equation (10) are eliminated. In the vectors case, only lines are eliminated.

We are now interested in controlling the forward velocity u and the angular velocity r by actuating in the horizontal thrusters $P1$ and $P2$. Thus, we may define the error vector $e_h \in \mathbb{R}^3$ as the difference between the velocity reference v_{ref} and the relative velocity v_r for the components along the surge and yaw. Thus, we define the matrix S_h as the selection matrix shown below:

$$e_h = S_h v_{rh} - v_{refh} = \begin{bmatrix} 1 & 0 & 0 \\ 0 & 0 & 1 \end{bmatrix} \begin{bmatrix} u \\ v \\ r \end{bmatrix} - \begin{bmatrix} u_{ref} \\ r_{ref} \end{bmatrix} = \begin{bmatrix} u - u_{ref} \\ r - r_{ref} \end{bmatrix} \tag{20}$$

Note that the lateral velocity error is always null since we do not want to control it and in fact we cannot.

The determination of this controller is similar in every step to the vertical velocity controller previously presented. The resulting expression of the control law is equal to equation (18). Only matrices and vectors of the simplified model are different.

Computing of the gain is similar to the previous section, where actuation saturations and maximum values of velocities are taken into account to define k_e and error saturation values.

3.3. Position Controller

3.3.1. Vertical Position

Unlike Aguiar and Hespanha (2007), we will deduce a controller that uses the velocity controller deduced in section 3.2.1. The architecture of the system will result in what is shown in Figure 3.

Velocity references (w_{ref} and q_{ref}) will be generated dynamically and will be applied to the vertical velocity controller. The use of this last controller allows the virtual decoupling of both linear and angular velocities.

FIGURE 3

Architecture of vertical position control.

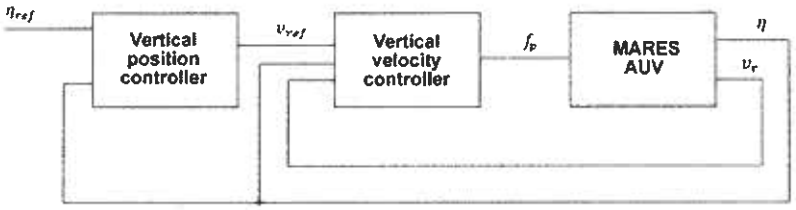

We expect that the vehicle reaches the depth reference z_{ref} and the pitch angle θ_{ref}, as illustrated in Figure 4.

To design this controller, we start by defining position errors in the vertical plane (see Figure 4).

$$e_z = \frac{1}{\cos\theta}(z - z_{ref}) \tag{21}$$

$$e_\theta = \theta - \theta_{ref} \tag{22}$$

These errors make it possible to define a position controller with proportional and integral gains. In fact, this will be constituted by two independent controllers of the depth and of the angle:

$$w_{ref} = -K_{pz}\, e_z - K_{iz}\int e_z\, dt \tag{23}$$

$$q_{ref} = -K_{p\theta}\, e_\theta - K_{i\theta}\int e_\theta\, dt \tag{24}$$

where $K_{pz}, K_{iz}, K_{p\theta}, K_{i\theta} \in \mathbb{R}^+$ are proportional and integral gains.

The determination of this controller aims to obtain an invariant behavior independent of the error values. However, integral terms in equations (23) and (24) depend directly on these errors. To illustrate this concept, we consider a constant error that leaves actuation to saturation during an interval of time. The maximum value of the velocity w would be reached and the actuation would continue in saturation. The bigger the error, the bigger the integral term due to the elapsed time and to error value. This behavior may be attenuated if the error is saturated. The integral component is reset upon saturation and activated when the error is no longer saturated:

$$\int e\, dt = 0,\ |e| > e_{max} \tag{25}$$

Controller gains must be determined considering velocity saturation values of the vertical velocity controller and error saturations.

Note that the main advantage of this architecture is to drive the error to zero in steady state, which could not be achieved by the approaches followed by Aguiar and Hespanha (2007) and Li (2009).

3.3.2. Line-Following Controller

The controller that will be designed in this subsection will make it possible to follow an imaginary straight line defined by two horizontal points (x_1, y_1) and (x_2, y_2). Considering the previous determined controllers, we may assume that this motion is independent of the vertical one. Therefore, it implies that the vehicle can follow a line and dive simultaneously, for instance.

The architecture of this controller is almost the same as the one defined in section 4.3.1. However, we must note that forward relative velocity is defined independently. It will not be generated by the position controller and may be modified along the trajectory.

To guarantee a high dynamic response of the system for any distance and any angle to the line, it is necessary to determine an approach and a proximity controller. The first one will be responsible for taking the vehicle closer to the line, while the second one will have the purpose of leading the error to zero in steady state. Switching between them must be done according to the distance using a hysteresis selector whose values need to be properly defined. The inclusion of the hysteresis selector is

FIGURE 4

Vertical motion in position control.

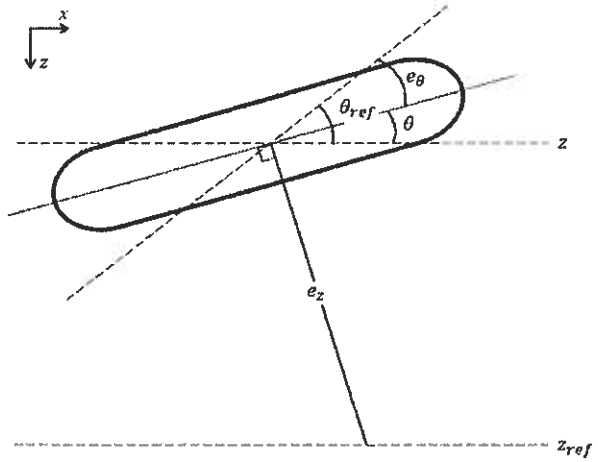

essential to avoid high frequency switching between controllers. In this work, we considered hysteresis threshold values of 5 and 10 m.

3.3.2.1. Approach controller

While imposing a forward velocity reference to the controller, it is necessary that its orientation (yaw angle ψ) enables an approach to the line. The minimum distance between the vehicle and the line is given by the segment that intersects the vehicle and is perpendicular to the line (Figure 5a). Thus, the approach to the line will be done perpendicularly to it.

Therefore, we define the equation of the straight line that we wish to follow as a function of the absolute position component x:

$$y_r(x) = mx + b \tag{26}$$

where $m = \frac{y_2 - y_1}{x_2 - x_1}$ and $b = y_1 - mx_1$.

Assuming that $u > 0$, we define the angle of the perpendicular to the line that we wish to follow as

$$\psi_p = \begin{cases} \psi_{ref} - \frac{\pi}{2}, & y \geq y_r \\ \psi_{ref} + \frac{\pi}{2}, & y < y_r \end{cases} \tag{27}$$

where $\psi_{ref} = \measuredangle((x_2, y_2), (x_1, y_1))$.

Thus, the error of the angle of the vehicle during the approach to the line is given by

$$e_\psi = \psi - \psi_p \tag{28}$$

Presented concepts are shown in Figure 5a.

The resulting control law follows:

$$r_{ref} = -K_{p\psi} e_\psi \tag{29}$$

where $K_{p\psi} \in \mathbb{R}^+$ is the proportional gain computed taking into account both the saturation of e_ψ and the saturation of yaw velocity reference r_{ref} in the horizontal velocity controller.

3.3.2.2. Proximity controller

With this controller, we intend to obtain a null distance to the line in steady state. To reach this goal, we introduce a proportional and an integral component of the distance error, which is given by

$$\begin{aligned} e_d &= -(y - y_r)\cos\left(\pi - \psi_{ref}\right) \\ &= (y - y_r)\cos\left(\psi_{ref}\right) \end{aligned} \tag{30}$$

To impose the following direction (from point 1 to point 2), it is also necessary to add a proportional term of the angle between the vehicle and the line. To satisfy this, we redefine the angle error:

$$e_\psi = \psi - \psi_{ref} \tag{31}$$

The control law results

$$\begin{aligned} r_{ref} = &-K_{p\psi} e_\psi - K_{pd} e_d \\ &- K_{id} \int e_d dt \end{aligned} \tag{32}$$

FIGURE 5

(a) Approach to the line; (b) in the proximity of the line.

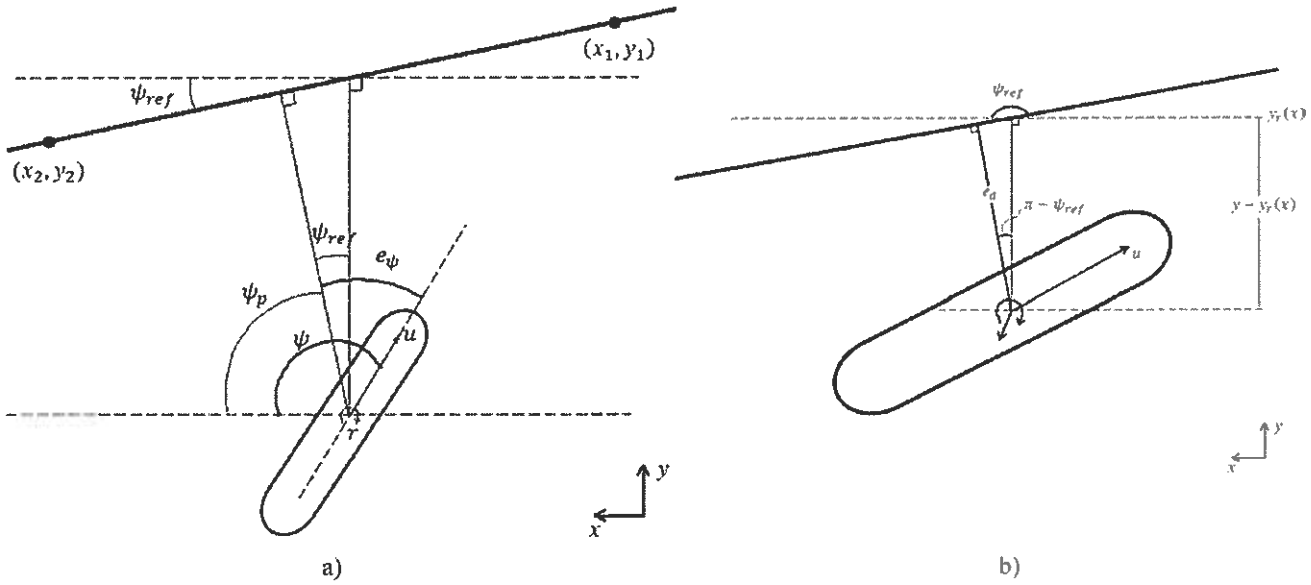

When there is a switch in the approach controller, the integration must be suspended and reset ($\int e_d\,dt = 0$).

Gains have to be computed in such a way that the $K_{p\psi}\,e_\psi$ is dominant and $K_{id}\int e_d\,dt$ does not overcome $K_{pd}\,e_d$, to have an asymptotical convergence of the error to zero. The integral term directly depends on time and indirectly depends on forward velocity and therefore these factors have to be taken into account to derive $K_{id}(u)$. In practice, the integral gain must be computed for different values of u. Error saturations of the horizontal velocity controller must also be accounted for.

It would be interesting if the vehicle could describe the same trajectory (relative to the fluid) during the line following, independently of the forward velocity u. Close to a given (x, y) position, the trajectory described by the vehicle during an infinitesimal interval of time may be considered as an arc of circumference with curvature $r_c(x, y)$. If this function is invariant, that is

$$r_c(x,y)|_{u=u_1} = r_c(x,y)|_{u=u_2} \tag{33}$$

with $u_1 \neq u_2$, then the trajectory will be invariant since the initial conditions are the same.

We may write

$$r_c(x,y) = \frac{u_1(t)}{r_1(t)} = \frac{u_2(t)}{r_2(t)} \tag{34}$$

where r_1 and r_2 are velocities of rotation after yaw for velocities u_1 and u_2, respectively.

Control laws for both cases are given by

$$r_{ref}|_{u=u_1} = -K_{p\psi}\,e_\psi - K_{pd}\,e_d - K_{id}\int e_d\,dt \tag{35}$$

$$r_{ref}|_{u=u_2} = -K'_{p\psi}\,e_\psi - K'_{pd}\,e_d - K'_{id}\int e_d\,dt \tag{36}$$

Using equations (34), (35) and (36), we easily conclude that gain values are related as follows:

$$K'_{p\psi} = \frac{u_2}{u_1}K_{p\psi};\quad K'_{pd} = \frac{u_2}{u_1}K_{pd};\quad K'_{id}(u) = \frac{u_2}{u_1}K_{id}(u) \tag{37}$$

3.3.3. Hovering Controller

Considering that the flow velocity of the involving fluid v_f is sufficiently small compared to that of the MARES, in such a way that it can move in all directions, we determine a controller that supplies the horizontal velocity controller with a reference. The architecture adopted is similar to the one presented for the vertical position controller in Figure 3. It will be divided into two basic controllers: an approach controller similar to those presented in previous subsection and a proximity controller that allows the vehicle to stabilize in the target, with no motion regarding to an earth-fixed referential. The selection of controller remains the same as in the previous subsection: a hysteresis selector is used to properly decide which controller must be activated.

3.3.3.1. Approach controller

To guarantee that the system has a good behavior for a large range of operations, an approach is performed before the immobilization maneuver. This is achieved at an externally defined forward velocity reference u_{ref}, correcting the angle between the orientation of the vehicle and the straight formed by the reference point (x_{ref}, y_{ref}) and the vehicle, along the trajectory. Thus, it leads to

$$\psi_{ref} = \measuredangle\big((x,y),(y_{ref},x_{ref})\big) \tag{38}$$

The control law is then given by

$$r_{ref} = -K_{p\psi}\,e_\psi \tag{39}$$

where $e_\psi = \psi - \psi_{ref}$ and $K_{p\psi} \in \mathbb{R}^+$.

3.3.3.2. Proximity controller

Taking into account that MARES only has four DOF, in steady-state, the vehicle must be parallel to the current flow. In Figure 6, we show the vehicle with a given reference (x_{ref}, y_{ref}), in a fluid with non null linear velocity v_f.

The y_s-component of fluid velocity in the vehicle referential is given by e_{v_f}:

$$e_{v_f} = [0 \quad 1 \quad 0]\cdot J^T(\psi)\cdot v_f \tag{40}$$

whose expression, for $r \approx 0$ and $p \approx 0$, may be approximated by

$$e_{v_f} \approx [0 \quad 1 \quad 0]\cdot J^T(\psi)\cdot \dot{\eta} \tag{41}$$

where we recall that $\dot{\eta}$ is the time derivative of the absolute position in the inertial frame (earth fixed).

FIGURE 6

Horizontal motion of MARES with non-null current.

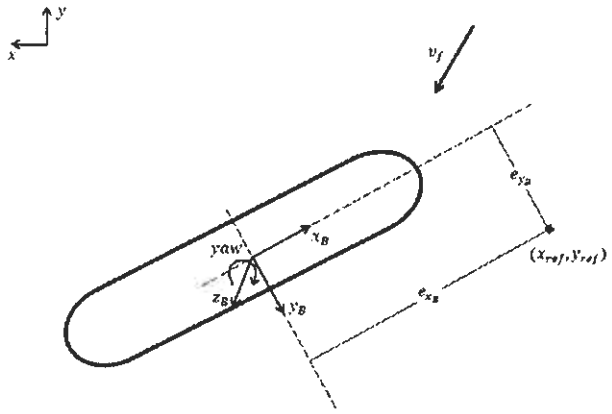

The error distance vector (e_{xB}, e_{yB}) referred to the body-fixed frame is given by the following expression:

$$\begin{bmatrix} e_{x_B} \\ e_{y_B} \\ 0 \end{bmatrix} = J^T \cdot \left(\begin{bmatrix} x \\ y \\ 0 \end{bmatrix} - \begin{bmatrix} x_{ref} \\ y_{ref} \\ 0 \end{bmatrix} \right) \quad (42)$$

The effect of the longitudinal error e_{xB} must be reflected directly in the forward velocity reference u_{ref}. On the other hand, the lateral component of the fluid velocity e_{v_f} and the lateral component of the distance error e_{yB} must be reflected in the yaw velocity reference r_{ref}. Therefore, we obtain the following control laws:

$$u_{ref} = -K_{px}\, e_{x_B} - K_{ix} \int e_{x_B} dt \quad (43)$$

$$r_{ref} = -K_{pv}\, e_{v_f} - K_{py}\, e_{y_B} - K_{iy} \int e_{y_B} dt \quad (44)$$

where $K_{px}, K_{ix}, K_{pv}, K_{py}, K_{iy} \in \mathbb{R}^+$.

It is important to refer that, for expression (44), the compensation effect of the flow, given by $K_{pv}\, e_{v_f}$, must be dominant relatively to others, guaranteeing that the fluid velocity does not induce an excessive lateral force. In other words, the yaw angle ψ of the vehicle must be opposed to the flow ($\psi \approx \measuredangle(v_f, u_f) + \pi$), with small deviations. So, proportional and integral gains must be computed considering these facts, as well as the velocity error saturations of the horizontal velocity controller.

Integration components of equations (43) and (44) must be restarted whenever the approach controller is activated.

4. Experimental and Simulation Results

4.1. System Description

The position of the AUV MARES is estimated using pressure and tilt sensors. From the pressure sensor, the depth is directly obtained by a linear relationship with accuracy in the magnitude of one centimeter. Tilt sensors provide the angles of heading, roll and pitch, with accuracies better than 0.5°. Horizontal position is estimated through acoustic techniques: MARES emits an acoustic signal to two buoys placed in the mission area, which in turn respond to the AUV. Combining the data about the depth and the measurement of the time of flight of the acoustic waves, it is possible to compute the distance to the buoys and consequently estimate the horizontal position. Since the determination of distances using acoustic methods works at low frequencies, dead-reckoning techniques are used between consecutive observations. Moreover, this kind of localization is affected by low frequency noise with a standard deviation of about 1.5 m.

The computational device is composed by a PC104 stack capable of running Linux. It interfaces with all sensors in the vehicle and provides actuation references to the thrusters and order emission of acoustic signal for localization. Controllers were developed in the referred programming language, with update and actuation cycles of 100 ms. A more detailed description of the system is given by Matos and Cruz (2009).

4.2. Validation of the Model

Since we are not able to perform hydrodynamic tests under experimental environments due to material constraints, an interesting alternative is estimating some of the coefficients while performing missions. To achieve this, it is necessary to know the force applied by each thruster, which may be indirectly determined by the observation of the electrical variables of the motors. A direct and accurate relationship may be extracted from the analysis of the current. However, MARES is not yet equipped with current sensors, whereby we may perform a voltage analysis in steady state, although it is less accurate than current analysis. Through experimental tests in bollard conditions using a dynamometer and an adjustable power supply, we have found the relationship presented in the next figure. We show the force applied in both the direct (positive) and

reverse (negative) thrusts, since the responses are not symmetrical, as far as the origin and geometrical characteristics of the thrusters and its propeller are concerned.

To validate and correct the model of MARES, experimental tests were performed. They were carried out in the Douro River, near Porto, in the north of Portugal. During these tests, internal data of controllers, supply voltage, references of thrusters and localization data were collected. Among other experiments, we have estimated the value of surge and heave drag in steady state.

First, the horizontal velocity controller was set to a linear motion at constant forward velocity u_{ref} = 1 m/s and θ = 0. The flow effect was neglected since its velocity is much smaller than that of the vehicle. The filtered data of the absolute position time derivative give an average velocity of $u \approx$ 0.95 m/s.

For this velocity, we estimate that the force of horizontal thrusters is $F_{p1} \approx F_{p2} \approx 4.7$ N based on the experimental data collected from the steady state of thrusters (Figure 7). For steady state with constant forward velocity, we deduce

$$X_{u|u|} = -\frac{F_{p1} + F_{p2}}{u|u|} \approx -10\ \mathrm{kg \cdot m^{-1}} \quad (45)$$

The drag component for the surge motion was clearly underestimated due to the drag coefficient, which depends on the roughness of the hull and on the diameter/length relationship. As we are not able to measure this variable adequately, we initially took the experimental value obtained by Prestero (2001). The value obtained experimentally for $X_{u|u|}$ implies a maximum forward velocity $u_{max} \approx 2$ m/s for the model that incorporates this value, which is close to the observed real behavior.

To determine the heave drag, a vertical velocity controller was set to dive at constant velocity w_{ref} = 0.4 m/s. In steady state ($\dot{v}_r = 0_{6\times1}$), the heave velocity was constant and equal to w = 0.36 m/s. The collection of data related to the voltage applied to vertical thrusters makes it possible to estimate the applied force: $F_{p3} \approx F_{p4} \approx 7.5$ N. Therefore, for steady state with constant diving velocity, it is possible to determine the drag coefficient, as demonstrated below:

$$Z_{w|w|} = -\frac{F_{p3} + F_{p4}}{w|w|} \approx 1.22 \cdot 10^{2}\ \mathrm{kg \cdot m^{-1}} \quad (46)$$

This result is very close to the theoretical one.

FIGURE 7

Force applied by the thrusters as a function of the voltage. Markers represent effectively measured points.

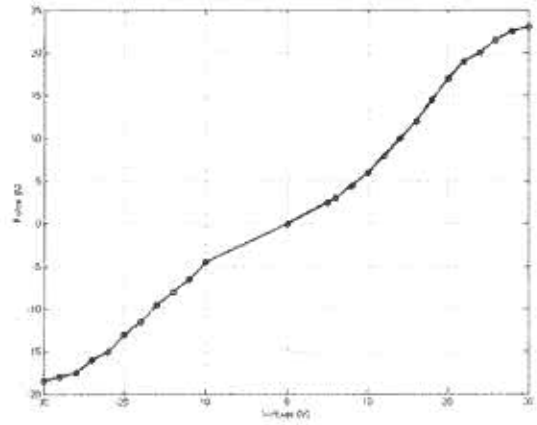

4.3. Controller Operation

To test the designed controllers, we implemented a simulation environment of the vehicle. The complete model with six DOF, deduced in section 2, given by the nonlinear differential equation (10), is simulated through the Matlab Simulink. Environmental constraints and limitations are recreated: high uncertainty and low frequency noise due to the horizontal acoustic positioning (Borenstein et al., 1996; Cruz and Matos, 2008) are the most important characteristics. The remaining state variables, such as depth, yaw and pitch angles, are directly read from relative sensors and are assumed to be precise enough and not affected by noise.

In some cases, we intend to validate controllers and the dynamical model through the comparison of results. Missions were performed considering the theoretically estimated model for expressions of controllers.

4.3.1. Vertical Motion

Aiming to collect relevant data, we designed a mission where the vehicle dives at constant velocity w = 0.5 m/s at θ = 0 until reaching 1.5 m of depth. At this point, the depth reference is kept constant while the pitch reference sequentially assumes several values: θ_{ref} = 10°, −10°, 20°, −20°. The response of the system is shown in Figure 8.

These results are satisfactory and allow the validation of the vertical

FIGURE 8

Experimental and simulation results for (a) depth z and (b) pitch angle θ.

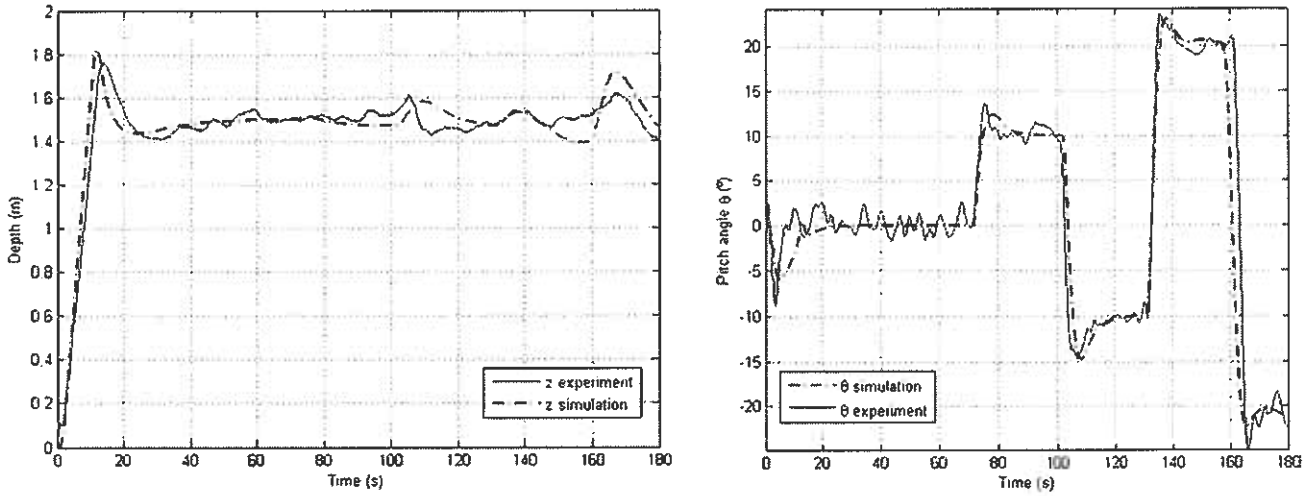

(a) (b)

velocity and position controllers. The model is also partially validated, since the experimental and simulated responses are very similar.

It should be noted that the vehicle remains at a fairly close distance to the surface, thus leading to disturbances in the system caused by small waves and wind. Nevertheless, controllers prove to be robust with very small deviations from their references: 5 cm for depth and 2° for pitch angle, before the variation of the pitch reference (t < 70 s). Though varying the pitch reference affects the depth of the center of gravity (as shown in Figure 8a), the deviation remains reduced even when the pitch reference varies from +20° to -20°. In fact, experimental data present maximal deviations of about 10 cm even in the presence of small delays from the sensor data.

Also, results obtained for pitch show the accuracy introduced by the controllers. Although low frequency noise affects the system, through small variations of the angle, the behavior of the system proves to be stable and accurate. As shown in Figure 8b, abrupt variations of the reference leads to small overshoots and small deviations (2°), as well.

4.3.2. Line Following

In section 3, we derived several controllers to control both horizontal and vertical velocities and positions. In the last subsection, the performance of the vertical position controller was demonstrated. Since the system is well behaved in the vertical plane, horizontal controllers may be combined with the vertical ones. Together, the controllers of vertical position and line following were used. The first is used to maintain the depth and the pitch angle at given references, while the second is used to approach and track an imaginary horizontal line.

In the next figures, we show the real trajectory of the AUV, as well as the filtered data of the velocity during the approach to the line, computed as the time derivative of the absolute position of the MARES AUV.

As we can see, the trajectory is affected by noise, particularly in the approach to the reference line, due to the acoustic localization. At the moment, we are not in condition to verify if all collected points are correct due to the uncertainties of the navigation system. However, it is possible to conclude that the general behavior is satisfactory. Obviously, the operation of this controller can be improved using a more accurate positioning system. Nevertheless, we may conclude that the controller is robust to the intrinsic noise of the positioning system.

The performance of the horizontal velocity controller may also be evaluated in Figure 9b. Note that the small variations around the expected value may be justified by the fact that velocity is indirectly calculated using the time derivative of the (noisy) position.

Through simulation, we obtain errors of the distance to the line as a function of time for distinct velocities (Figure 10). This makes it possible to compare trajectories in the approach to the line. It should be noted that noise was not simulated in the horizontal position because we are only interested in observing the behavior for different surge velocities.

Though it is not exactly the same, errors are very similar, which allows us

FIGURE 9

(a) Estimated described trajectory for line following (the maneuver starts at (–27; –47)). (b) Forward velocity.

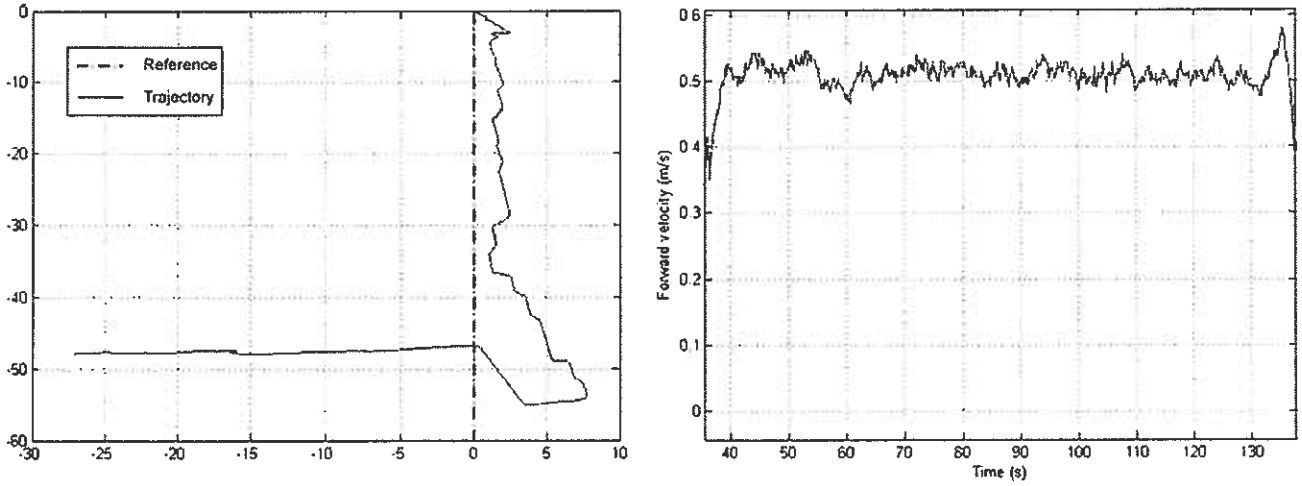

(a) (b)

to conclude that trajectories of the vehicle for different velocities are also very close. Note that during the approach phase of the maneuver, the line tracking error is arbitrarily set to zero.

5. Conclusions

This paper proposes a methodology for the design of controllers for elementary maneuvers of the small size AUV MARES. This vehicle was developed at the University of Porto and is able to execute independent motions in the vertical and horizontal planes due to the configuration of its thruster.

Based on the geometric characteristics of MARES, we present a simplified six DOF dynamic model of the vehicle motion that takes into account the most relevant forces and torques. This model is based on the kinematics and dynamics of a submerged rigid body, and its derivation follows the standard approach presented in the literature.

Regarding the control of the vehicle, we start with the design of velocity controllers for decoupled modes of operation. These controllers take into account the nonlinearities of the vehicle dynamic model and their design is based on the Lyapunov direct method, which intrinsically assures their stability. We then embed these controllers in outer feedback loops to allow the implementation of elementary maneuvers, such as the following of a horizontal line or the stationary control of the AUV at a given point. This approach may be easily extended or adapted to other underwater vehicles with different characteristics and to most mobile robots, as well.

We considered decoupled controllers for the horizontal and vertical motions based on two major reasons. The first one is directly related to the elementary maneuvers that our vehicle is able to execute. The second one arises from the fact that the vertical motion is commanded by two thrusters instead of fins, therefore greatly reducing the coupling of vertical and horizontal motions. Furthermore, this approach significantly simplifies the derivation of control laws and the analysis of their performance and stability characteristics.

FIGURE 10

Comparison between errors for different forward velocities.

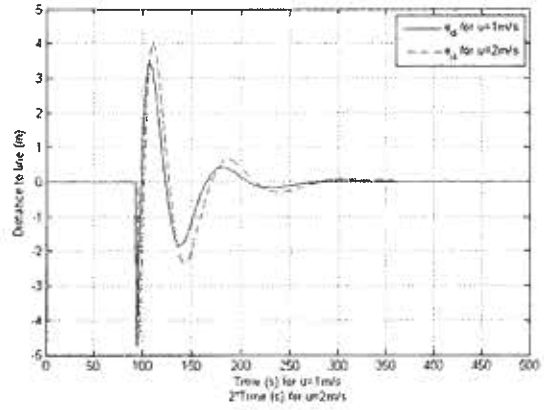

Finally, we present results both from realistic simulations and from real experiments that validate our approach. Controllers exhibit robust behaviors as well as good performances in the presence of intrinsic and environmental disturbances, even with inaccuracies in the values of the model coefficients.

From a practical point of view, these experimental results prove that the consideration of an approximate model of the vehicle dynamics together with the derivation of control laws that takes into account its major nonlinearities can be sufficient to achieve adequate performances.

Acknowledgments

The first author was supported by the Portuguese Foundation for Science and Technology through the Ph.D. scholarship SFRH/BD/60522/2009.

Lead Author:

Bruno Ferreira
INESC, Porto; University of Porto, Portugal
Candidate for Ph.D. in Electrical Engineering, 2013
E-mail: bm.ferreira@fe.up.pt

Appendix

$M_{RB} = diag(m, m, m, I_{xx}, I_{yy}, I_{zz})$

where I_{ii} is the moment of inertia after the i-axis, and

$$C_{RB} = \begin{bmatrix} 0 & -mr & mq & 0 & 0 & 0 \\ mr & 0 & -mp & 0 & 0 & 0 \\ -mq & mp & 0 & 0 & 0 & 0 \\ 0 & 0 & 0 & 0 & I_{zz}r & -I_{yy}q \\ 0 & 0 & 0 & -I_{zz}r & 0 & I_{xx}p \\ 0 & 0 & 0 & I_{yy}q & -I_{xx}p & 0 \end{bmatrix}$$

considering that the body-fixed referential coincides with the center of gravity of the body and that the products of inertia (I_{ij} for $i \neq j$) are negligible.

$$M_A = -\begin{bmatrix} X_{\dot{u}} & 0 & 0 & 0 & X_{\dot{q}} & 0 \\ 0 & Y_{\dot{v}} & 0 & Y_{\dot{p}} & 0 & Y_{\dot{r}} \\ 0 & 0 & Z_{\dot{w}} & 0 & Z_{\dot{q}} & 0 \\ 0 & K_{\dot{v}} & 0 & K_{\dot{p}} & 0 & 0 \\ M_{\dot{u}} & 0 & M_{\dot{w}} & 0 & M_{\dot{q}} & 0 \\ 0 & N_{\dot{v}} & 0 & 0 & 0 & N_{\dot{r}} \end{bmatrix}$$

where A_k is the added mass coefficient of the force induced along A by the acceleration along k.

$$C_A(v) = \begin{bmatrix} 0 & 0 & 0 & 0 & C_A^{15} & C_A^{16} \\ 0 & 0 & 0 & -C_A^{15} & 0 & C_A^{26} \\ 0 & 0 & 0 & -C_A^{16} & -C_A^{26} & 0 \\ 0 & C_A^{15} & C_A^{16} & 0 & C_A^{45} & C_A^{46} \\ -C_A^{15} & 0 & C_A^{26} & -C_A^{45} & 0 & C_A^{56} \\ -C_A^{16} & -C_A^{26} & 0 & -C_A^{46} & -C_A^{56} & 0 \end{bmatrix}$$

where

$$C_A^{15} = -Z_{\dot{w}}w - Z_{\dot{q}}q$$
$$C_A^{16} = Y_{\dot{v}}v + Y_{\dot{p}}p + Y_{\dot{r}}r$$
$$C_A^{26} = -X_{\dot{u}}u - X_{\dot{q}}q$$
$$C_A^{45} = -Y_{\dot{r}}v - N_{\dot{r}}r$$

$$C_A^{46} = X_{\dot{q}} u + Z_{\dot{q}} w + M_{\dot{q}} q$$
$$C_A^{56} = -Y_{\dot{p}} v - K_{\dot{p}} p$$

$$D_v(v_r) = -\begin{bmatrix} X_{u|u|}|u| & 0 & 0 & 0 & X_{q|q|}|q| & 0 \\ 0 & Y_{v|v|}|v| & 0 & Y_{p|p|}|p| & 0 & Y_{r|r|}|r| \\ 0 & 0 & Z_{w|w|}|w| & 0 & Z_{q|q|}|q| & 0 \\ 0 & K_{v|v|}|v| & 0 & K_{p|p|}|p| & 0 & 0 \\ M_{u|u|}|u| & 0 & M_{w|w|}|w| & 0 & M_{q|q|}|q| & 0 \\ 0 & N_{v|v|}|v| & 0 & 0 & 0 & N_{r|r|}|r| \end{bmatrix}$$

where $A_{i|i|}$ is the coefficient of the force induced along A by the i velocity.

$$p = \begin{bmatrix} 1 & 1 & 0 & 0 \\ 0 & 0 & 0 & 0 \\ 0 & 0 & 1 & 1 \\ 0 & 0 & 0 & 0 \\ z_{p1} & z_{p2} & -x_{p3} & -x_{p4} \\ -y_{p1} & -y_{p2} & 0 & 0 \end{bmatrix}; \qquad f_p = \begin{bmatrix} F_{p1} \\ F_{p2} \\ F_{p3} \\ F_{p4} \end{bmatrix}$$

where x_{pi}, y_{pi} and z_{pi} are the positions along x, y and z of the thruster i.

TABLE A.1

Moments of inertia.

Parameter	Valor [kg m^2]	Description
I_{xx}	$1.55 \cdot 10^{-1}$	Moment of inertia along x_B
I_{yy}	$4.73 \cdot 10^{0}$	Moment of inertia along y_B
I_{zz}	$4.73 \cdot 10^{0}$	Moment of inertia along z_B

TABLE A.2

Added mass coefficients.

Parameter	Value	Units
$X_{\dot{u}}$	$-1.74 \cdot 10^{0}$	kg
$Y_{\dot{v}}$	$-4.28 \cdot 10^{1}$	kg
$Z_{\dot{w}}$	$-4.12 \cdot 10^{1}$	kg
$K_{\dot{p}}$	$-8.61 \cdot 10^{-3}$	kg m^2
$M_{\dot{q}}$	$-6.07 \cdot 10^{0}$	kg m^2
$N_{\dot{r}}$	$-6.40 \cdot 10^{0}$	kg m^2
$X_{\dot{q}}$	$-3.05 \cdot 10^{-2}$	kg m
$Y_{\dot{p}}$	$3.05 \cdot 10^{-2}$	kg m
$K_{\dot{v}}$	$3.05 \cdot 10^{-2}$	kg m
$M_{\dot{u}}$	$-3.05 \cdot 10^{-2}$	kg m
$Y_{\dot{r}}$	$1.13 \cdot 10^{-1}$	kg m
$Z_{\dot{q}}$	$-1.23 \cdot 10^{-1}$	kg m
$M_{\dot{w}}$	$-1.23 \cdot 10^{-1}$	kg m
$N_{\dot{v}}$	$1.13 \cdot 10^{-1}$	kg m

TABLE A.3

Viscous damping coefficients.

Parameter	Value	Units
$X_{u\|u\|}$	$-4.05 \cdot 10^{0}$	kg m^{-1}
$Y_{v\|v\|}$	$-1.16 \cdot 10^{2}$	kg m^{-1}
$Z_{w\|w\|}$	$-1.16 \cdot 10^{2}$	kg m^{-1}
$K_{p\|p\|}$	$-7.02 \cdot 10^{-4}$	kg m^2
$M_{q\|q\|}$	$-1.56 \cdot 10^{1}$	kg m^2
$N_{r\|r\|}$	$-1.25 \cdot 10^{1}$	kg m^2
$X_{q\|q\|}$	$-4.84 \cdot 10^{-2}$	kg m
$Y_{p\|p\|}$	$4.84 \cdot 10^{-2}$	kg m
$M_{u\|u\|}$	$-2.11 \cdot 10^{-1}$	kg
$K_{v\|v\|}$	$211 \cdot 10^{-1}$	kg
$Y_{r\|r\|}$	$1.83 \cdot 10^{0}$	kg m
$Z_{q\|q\|}$	$-5.95 \cdot 10^{0}$	kg m
$M_{w\|w\|}$	$-8.26 \cdot 10^{0}$	kg
$N_{v\|v\|}$	$2.13 \cdot 10^{0}$	kg

TABLE A.4

Coordinates of the positions of thrusters.

Parameter	Value [m]
x_{p1}	$-7.47 \cdot 10^{-1}$
y_{p1}	$-1.08 \cdot 10^{-1}$
z_{p1}	$-1.20 \cdot 10^{-3}$
x_{p2}	$-7.47 \cdot 10^{-1}$
y_{p2}	$1.08 \cdot 10^{-1}$
z_{p2}	$-1.20 \cdot 10^{-3}$
x_{p3}	$-4.21 \cdot 10^{-1}$
y_{p3}	0
z_{p3}	0
x_{p4}	$4.34 \cdot 10^{-1}$
y_{p4}	0
z_{p4}	0

References

Aguiar, A.P., Hespanha, J.P. 2004. Logic-based switching control for trajectory-tracking and path-following of underactuated autonomous vehicles with parametric modeling

uncertainty. In: Proceedings of the 2004 American Control Conference. Vols. 1-6. pp. 3004-3010. New York: IEEE.

Aguiar, A.P., Hespanha, J.P. 2007. Trajectory-tracking and path-following of underactuated autonomous vehicles with parametric modeling uncertainty. IEEE Trans Automat Contr. 52(8):1362-1379.

Borenstein, J., Everett, H.R., Feng, L. 1996. Navigating Mobile Robots: Systems and Techniques. Ann Arbor, MI: A. K. Peters, Ltd. 225 pp.

Cruz, N., Matos, A. 2008. The MARES AUV, a modular autonomous robot for environment sampling. In: Oceans 2008. Vols. 1-4. pp. 1996-2001. New York: IEEE.

Dunbar, W.B., Murray, R.M. 2002. Model predictive control of coordinated multi-vehicle formations. In: Proceedings of the 41st IEEE Conference on Decision and Control. Vols. 1-4. pp. 4631-4636. New York: IEEE.

Evans, J., Nahon, M. 2004. Dynamics modeling and performance evaluation of an autonomous underwater vehicle. Ocean Eng. 31(14-15):1835-1858.

Ferreira, B. 2009. Modelação e controlo de veículo submarino com quatro graus de liberdade. department of electronic and computer engineering. M.Sc. thesis, University of Porto, Porto, Portugal. 168 pp.

Ferreira, B., Pinto, M., Matos, A., Cruz, N. 2009. Modeling and motion analysis of the MARES autonomous underwater vehicle. In: OCEANS. I. MTS. Biloxi: MTS, IEEE.

Fossen, T.I. 1991. Nonlinear modelling and control of underwater vehicle. Ph.D. thesis, Department of Engineering Cybernetics, The Norwegian Institute of Technology, Trondheim, Norway.

Fossen, T.I. 1995. Guidance and Control of Ocean Vehicles. Chichester: John Wiley & Sons.

Healey, A.J., Lienard, D. 1993. Multivariable sliding mode control for autonomous diving and steering of unmanned underwater vehicles. IEEE J Oceanic Eng. 18(3):327-339.

Hoerner, S.F. 1965. Fluid-Dynamic Drag: Practical Information on Aerodynamic Drag and Hydrodynamic Resistance. Bakersfield, CA: Hoerner.

Khalil, H.K. 2002. Nonlinear Systems. Upper Saddle River, NJ: Prentice-Hall.

Li, Z., Sun, J., Oh, S. 2009. Design, analysis and experimental validation of a robust nonlinear path following controller for marine surface vessels. Automatica. 45(7):1649-1658.

Matos, A., Cruz, N. 2009. MARES—navigation, control and on-board software. In: Underwater Vehicles, ed. Inzartsev, A. V., 594. Austria: Intech.

Ogata, K. 1997. Modern Control Engineering. New Jersey: Prentice Hall International.

Prestero, T. 2001. Verification of a six-degree of freedom simulation model for the REMUS autonomous underwater vehicle. M.Sc. thesis, Mechanical Engineering, Massachussets Institute of Technology, Cambridge. 128 pp.

Siegwart, R., Nourbakhsh, I.R. 2004. Introduction to Autonomous Mobile Robots. Cambridge, Massachusetts: The MIT Press.

Silvestre, C., Pascoal, A., Kaminer, I. 2002. On the design of gain-scheduled trajectory tracking controllers. Int J Robust and Nonlinear Control. 12(9):797-839.

Slotine, J.-J. E., Li, W. 1991. Applied Nonlinear Control. Upper Saddle River: Prentice Hall.

Song, F., An, E., Smith, S.M. 2002. Design robust nonlinear controllers for autonomous underwater vehicles with comparison of simulated and at-sea test data. Journal of Vibration and Control. 8(2):189-217.

Triantafyllou, M.S., Hover, F.S. 2003. Maneuvering and Control of Marine Vehicles. Cambridge, MA: Department of Ocean Engineering, Massachusetts Institute of Technology. 152 pp.

Tyagi, A., Sen, D. 2006. Calculation of transverse hydrodynamic coefficients using computational fluid dynamic approach. Ocean Engineering. 33(5-6):798.

van de Ven, P.W.J., Flanagan, C., Toal, D. 2005. Neural network control of underwater vehicles. Pergamon Press, Inc. Eng Appl Artif Intell. 18(5):533-547.

White, F.M. 2008. Fluid Mechanics. Boston: McGraw-Hill/Higher Education.

Yuh, J. 1994. Learning control for underwater robotic vehicles. IEEE Control Syst Mag. 14(2):39-46.